

Accepted to the Astrophysical Journal on 2002 December 12

## VLBI imaging of the RS CVn binary star system HR 5110

R. R. Ransom, N. Bartel and M. F. Bietenholz

*Department of Physics and Astronomy, York University*

*4700 Keele St., Toronto, Ontario, Canada M3J 1P3*

rransom@yorku.ca, bartel@yorku.ca, michael@polaris.phys.yorku.ca

M. I. Ratner, D. E. Lebach and I. I. Shapiro

*Harvard-Smithsonian Center for Astrophysics*

*60 Garden St., Cambridge, MA 02138*

mratner@cfa.harvard.edu, dlebach@cfa.harvard.edu, ishapiro@cfa.harvard.edu

and J.-F. Lestrade

*Observatoire de Paris/DEMIRM*

*77 av. Denfert Rochereau, F-75014 Paris, France*

lestrade@mesioa.obspm.fr

### ABSTRACT

We present VLBI images of the RS CVn binary star HR 5110 (=BH CVn; HD 118216), obtained from observations made at 8.4 GHz on 1994 May 29/30 in support of the NASA/Stanford Gravity Probe B project. Our images show an emission region with a core-halo morphology. The core was  $0.39 \pm 0.09$  mas (FWHM) in size, or  $66\% \pm 20\%$  of the  $0.6 \pm 0.1$  mas diameter of the chromospherically active K subgiant star in the binary system. The halo was  $1.95 \pm 0.22$  mas (FWHM) in size, or  $1.8 \pm 0.2$  times the  $1.1 \pm 0.1$  mas separation of the centers of the K and F stars. (The uncertainties given for the diameter of the K star and its separation from the F star each reflect the level of agreement of the two most recent published determinations.) The core increased significantly in brightness over the course of the observations and seems to have been the site of flare activity that generated an increase in the total flux density of  $\sim 200\%$  in 12 hours. The fractional circular polarization simultaneously decreased from  $\sim 10\%$  to 2.5%.

*Subject headings:* binaries: close — radio continuum: stars — stars: activity — stars: imaging — stars: individual (BH CVn) — techniques: interferometric

## 1. INTRODUCTION

HR 5110 (=BH CVn; HD 118216) is a close binary system with an orbital period of 2.61 days. The system consists of an F2 IV star (Slettebak 1955) and a K0 IV star (Little-Marenin et al. 1986). A tabulated list of selected properties and characteristics of HR 5110 is given in Table 1. HR 5110 is classified as a RS CVn (Hall 1976), primarily due to strong Ca II H and K emission from the chromosphere of the cooler K star (Conti 1967), although Little-Marenin et al. demonstrate that HR 5110 can also be considered an Algol system seen very close to pole-on (inclination,  $i \lesssim 13^\circ$ ; see Table 1). We adopt the *Hipparcos* distance for HR 5110 of  $44.5 \pm 1.3$  pc (Perryman 1997) throughout this paper.

Radio emission from HR 5110 is relatively strong and highly variable, with a flux density that ranges over approximately two orders of magnitude: Quiescent emission levels are in the 5–20 mJy range (Florkowski et al. 1985; Willson & Lang 1987), while flux densities as high as 460 mJy have been observed during intense flaring episodes (Feldman 1983). Model fitting of visibility data from past very-long-baseline interferometry (VLBI) observations of HR 5110 revealed source sizes ranging from 1.0 mas to more than 3.7 mas (Lestrade et al. 1984; Mutel et al. 1985; Little-Marenin et al. 1986).

Here we report on VLBI observations of HR 5110 made on 1994 May 29/30. The purpose of the observations was to obtain a position estimate of HR 5110, which was then a candidate guide star for the NASA/Stanford relativity gyroscope experiment, Gravity Probe B (GP-B; see, e.g., Turneure, Everitt, and Parkinson 1986). (HR 5110 was later rejected as the guide star in favor of a different RS CVn binary, HR 8703.) We describe our observations of HR 5110 in §2, and the data reduction and analysis procedures in §3. In §4, we present our VLBI images of HR 5110 as well as Gaussian model fits to the visibility data. In §5, we discuss our results and compare them to previous VLBI results for HR 5110. We summarize our conclusions in §6.

## 2. OBSERVATIONS

We made observations of HR 5110 with a global VLBI array of seven telescopes on 1994 May 29/30 (see Table 2). Our array had higher sensitivity and better spatial frequency ( $u$ - $v$ ) coverage than previous VLBI observations of this star system. Our total observing

time was approximately twelve hours. The observations were centered at a frequency of 8420 MHz ( $\lambda = 3.6$  cm), and were in right-hand circular polarization (RCP) only, since two of our antennas, Goldstone and Robledo, did not customarily support dual-polarization observations and a polarization measurement was not critical to our support of GP-B. Data were recorded with Very Long Baseline Array (VLBA) systems at the Very Large Array (VLA) and the VLBA-Hancock station and with Mark III recording systems in the Mark IIIA format at all other stations. The data were correlated at the Haystack Observatory.

We used the VLA as a stand-alone interferometer (in addition to using it as an element of our VLBI array) to monitor the variability of the total flux density and total circular polarization of HR 5110 over the course of our observations.

We observed HR 5110 in a repeating  $\sim 10$  minute cycle (including antenna slew time) with three extragalactic reference sources close on the sky ( $< 3^\circ$ ). Table 2 lists the reference sources observed as well as the dwell time per cycle on each source. We scheduled the observations this way so that we could employ phase referencing and thus determine a position for the radio emission region of HR 5110 in support of GP-B. However, once HR 5110 was dropped as the GP-B guide star, we turned our attention entirely to the structure and any relative motions of the emission source that we could discern from a single epoch of observations. Since the quality of images generated via hybrid mapping (see § 3) is superior to that of images generated via phase-reference mapping, we do not discuss our phase-referencing efforts in this paper.

### 3. DATA REDUCTION AND ANALYSIS

We analyzed the interferometric data from the VLA using NRAO’s Astronomical Image Processing System (AIPS) and following standard calibration procedures. The flux density calibrator source, 3C286, with flux density defined on the scale of Baars et al. (1977), was used to set the flux density scale for our VLA observations. We estimate a standard deviation of 5% for this absolute flux density calibration. We used the AIPS program DFTPL to plot the flux density of HR 5110, time-averaged in 10 minute intervals, over the course of the observing session.

We also used AIPS to reduce our VLBI data. The initial reduction, including fringe-fitting, editing, and preliminary amplitude calibration, was completed in the usual manner (see, e.g., Diamond 1995). The final calibration of the complex visibilities and the imaging of HR 5110 was done as follows:

- 1) We first imaged the reference sources using the hybrid mapping scheme for continuum

imaging described in Walker (1999). The initial model for the self-calibration of each source was a point source at the phase center, which is the point in the image corresponding to the position used during the correlation process, with flux density equal to the total RCP flux density found via the VLA. We used the resulting “final” images for the three reference sources to determine the antenna-based amplitude gains as a function of time over the course of the observations. For each antenna, the amplitude gains for the three reference sources agreed to within 5% at all times, so we used the average of these three gains to calibrate the HR 5110 data.

2) We then imaged HR 5110 using the same hybrid mapping scheme except that we performed no amplitude self-calibration since the star’s total flux density varied over the course of the observations. The initial model for the self-calibration in phase was a point source at the phase center. Note that our procedure discards information about the absolute position and motion of the source since the phase self-calibration serves to align the brightest feature with the phase center.

Flux densities measured with VLBI are not directly tied to the flux density scale of Baars et al. (1977) as are those measured with the VLA; rather, the VLBI flux density scale is based on system temperatures measured at each antenna over the course of an observing session. A comparison of the VLA-determined and VLBI-determined flux densities for the three extragalactic reference sources that we observed along with HR 5110 shows that the flux density on the VLBI scale is  $15\% \pm 5\%$  lower than the flux density on the VLA scale, where the uncertainty has been inferred from the ratios computed for each source separately. However, our CLEAN image of HR 5110 based on VLBI data from the full usable time range (see §4.2) contains  $\sim 50\%$  less flux density than the mean RCP flux density measured with the VLA during the same hours. After accounting for the  $15\% \pm 5\%$  difference in flux density scales, we attribute the remaining difference of  $\sim 35\% \pm 5\%$  between the VLBI CLEAN flux density and the mean VLA flux density to 1) the nonuniform sampling of the  $u$ - $v$  plane with time by our VLBI array over the course of the observations, and 2) the possible presence of structure that is at least partially resolved by even the shortest baselines in our VLBI array.

In addition to producing images of HR 5110, we also fit simple brightness-distribution models to the VLBI data (averaged into 30 minute bins) for each baseline using the AIPS program OMFIT. To describe the structure, we used first a one-component model consisting of a single elliptical Gaussian. The center of the elliptical Gaussian was fixed at the phase center. Second, we used a two-component model consisting of a circular Gaussian and an elliptical Gaussian. The centers of both the circular and elliptical Gaussians were fixed at the phase center. Third, we used a three-component model consisting of three circular Gaussians. The circular Gaussians were initially arranged east-west and the center of the

middle Gaussian was fixed at the phase center. OMFIT simultaneously estimates both the fit parameters and the time-varying antenna-based phase errors (i.e., it self-calibrates in phase). For want of any better estimate, the systematic contribution to the uncertainty in the value of each of the fit parameters for the full usable data set was estimated by monitoring the values of the parameter at each iteration of self-calibration. We chose as the standard error for each estimated parameter the root-sum-square of the statistical standard deviation of the fit and the maximum deviation of that parameter from its final value obtained during the iteration process. We also fit the three models described above separately to each of two subsets of the full usable data set corresponding approximately to the first half and the second half of the observations (see §4.2 for the exact time intervals for each subset). To obtain realistic estimates of the total, mostly systematic, errors for each subset, we repeated the model fit for even smaller subsets of the data. Specifically, we divided the data of each of the above subsets into halves of approximately equal duration and size (i.e., number of visibilities). In these cases, we give as the standard error for each estimated parameter for each subset, the root-mean-square (rms) of the deviations of the estimates for the two halves of that subset from the fit value for that same subset.

## 4. RESULTS

### 4.1. VLA Radio Light Curves

The VLA radio light curve, presented in Figure 1, shows that HR 5110 had relatively high radio emission during our 1994 May 29/30 observations. The flux density in RCP increased from  $\sim 33$  mJy to  $\sim 95$  mJy over the course of the observing period. The light curve also shows that the fractional circular polarization, defined as  $(R - L)/(R + L)$ , where  $R$  and  $L$ , respectively, represent the flux density in RCP and LCP, was  $9.6\% \pm 1.4\%$  for the first hour of observations, and decreased significantly to  $2.5\% \pm 0.6\%$  by the last hour. (As expected, the gain calibration for RCP and LCP agreed to within 0.2%, and therefore we believe that the uncertainty in fractional circular polarization is much smaller than the 5% standard error we estimated for the flux density calibration. The uncertainties quoted above are thus based solely on the scatter in the data points during the corresponding hour.) The sense of circular polarization, namely right circular, is the same as that observed for HR 5110 in July 1983 (Mutel et al. 1985). The constancy of the sense of circular polarization over time periods of  $\sim 10$  years has been observed in two other RS CVn systems (UX Arietis and HR 1099; see, e.g., Mutel et al. 1987). The degree of circular polarization in the last hour of our VLA observations is approximately that observed previously for HR 5110 in an active emission state ( $\sim 2\%$  with a flux density of  $\sim 140$  mJy at 4.9 GHz) by Mutel et al.

(1985). The observed trend, namely that the circular polarization decreases with increasing flux density, is in good agreement with that found for the RS CVn system HR 1099 (Mutel et al. 1987, 1998; Ransom et al. 2002).

## 4.2. VLBI Imaging and Model Fitting

The moderate to high flux density of HR 5110 on 1994 May 29/30 allowed us to detect the star on all VLBI baselines in most scans ( $\sim 93\%$ ) throughout our observations. However, for approximately one hour at both the start and end of our observations, the source was visible at only two of the seven antennas in our array. We were not able to reliably self-calibrate during these times and, therefore, the useful data set for the imaging process was reduced to a span of ten hours. The image made from these ten hours of data (Figure 2) shows that the emission source was extended in the east-west direction. Moreover, the concentration of contours around the brightness peak in the image indicates that there is a compact emission region within the extended region. This structure is consistent with a core-halo morphology. There is no clear indication of structure within the compact core.

The models that we fit to the visibility data yield a quantitative parameterization of the emission structure seen in the above image. The one-component model describes the most basic structure of the source. Its parameters are listed in Table 3. The  $1.66 \pm 0.21$  mas major axis size (full width at half-maximum: FWHM) and  $64^\circ \pm 8^\circ$  position angle (east of north) of the elliptical Gaussian is consistent with the footprint of the emission visible in the image. However, this model does not describe the compact region at the phase center. The two-component model provides a better fit to the data (i.e., has a 30% lower reduced chi-square). The size (FWHM) of the circular Gaussian converged to  $0.45 \pm 0.07$  mas, which approximately matches the compact region at the phase center in the image, while the position angle of the elliptical Gaussian converged to  $70^\circ \pm 8^\circ$ , equal within the errors to that of the elliptical Gaussian in the one-component model. However, the value of the axial ratio of the elliptical Gaussian converged to zero. Rather than describing a real feature that is completely unresolved in one dimension, the convergence is more plausibly related to: 1) the CLEAN beam of the interferometer array being highly elliptical and oriented approximately perpendicular to the major axis of the elliptical Gaussian; and 2) the relatively small number of antennas used for self-calibration. We therefore do not consider this model further. The best fit was obtained with the three-component model (37% lower reduced chi-square compared to the one-component model and 10% lower reduced chi-square compared to the two-component model) which is roughly consistent with all the structure in the image, namely a compact emission region with additional emission to both east and west. The

parameters for this model are listed in Table 4. The central component defines a compact region of size  $0.39 \pm 0.09$  mas (FWHM). The centers of the east and west components are separated from the center of the central component by only  $\sim 0.6$  times their own FWHMs. They lie along a line in the image plane at a position angle between approximately  $50^\circ$  and  $70^\circ$ . Based on the separation of the most distant parts of the half-maximum contours of its eastern and western components, we infer that this model defines an extended emission region  $1.95 \pm 0.22$  mas in diameter.

To investigate whether there were significant changes in the source structure of HR 5110 over the course of our observations, we divided the usable data set, as mentioned in §3, into two subsets of nearly equal duration: 1) 1994 May 29, 22:00 UT to May 30, 02:50 UT; and 2) 1994 May 30, 02:50 to 08:00 UT. We self-calibrated and imaged the data from each interval independently using the techniques described in §3. The resulting images are shown in Figure 3. Both images are roughly consistent with the image from the entire data set; i.e., they show a compact core surrounded by an extended halo. We also obtained satisfactory fits of one-component and three-component Gaussian models to the visibility data for each time interval. The results for the one-component models are given in rows 2 and 3 of Table 3, and those for the three-component models are given in rows 2 and 3 of Table 4. For interval 1, the three-component model fits the data better (i.e., has a 30% lower reduced chi-square) than the one-component model. For interval 2, no significant improvement (in reduced chi-square) is found with the three-component model in comparison to the one-component model. The three-component models for intervals 1 and 2 are very similar to the corresponding model for the full time range; i.e., the components lie along a position angle between approximately  $50^\circ$  and  $70^\circ$ , and define an emission region  $\sim 2.0$  mas in diameter (FWHM). However, while the flux densities of the western and eastern components remained constant within their standard errors from interval 1 to interval 2, the flux density of the central component increased by  $13.2 \pm 5.2$  mJy ( $92\% \pm 36\%$ ). In addition, there was an increase of  $22^\circ \pm 14^\circ$  from interval 1 to interval 2 in the position angle of the elliptical Gaussian in the one-component model. This change may be indicative of a small “rotation” in the source structure. However, the evidence for rotation is inconclusive for two reasons: First, no such rotation is indicated by our three-component models. Second, our limited  $u$ - $v$  coverage results in significant changes in the size and orientation of the beam of the interferometer array from interval 1 to interval 2. The fact that the beam computed for the full set of usable data more closely resembles the beam for interval 1 than that for interval 2 may explain why our estimates for almost all the model parameters for the full data set are closer to the corresponding estimates for interval 1 than to those for interval 2. If so, the differences in the beams for the two intervals may also be contributing significant systematic errors to the apparent changes in the parameters for the two intervals. Nevertheless, we doubt that such systematic errors account for all of

the apparent changes.

## 5. DISCUSSION

The images of the HR 5110 emission source from our 1994 May 29/30 observations show a compact region surrounded by an extended, elongated region. How do the sizes of these regions compare to the separation of the stellar components of the HR 5110 binary system and the diameters of the stars themselves? The  $1.95 \pm 0.22$  mas angular size we estimated for the extended region from the parameters of the two outer components in our three-component model (fit to the full set of usable data) corresponds to a linear size of  $(1.3 \pm 0.1) \times 10^{12}$  cm and indicates that the extended region was  $1.8 \pm 0.2$  times larger than the separation<sup>1</sup> of the centers of the K and F stars and  $3.3 \pm 0.8$  times larger than the diameter<sup>2</sup> of the chromospherically active K star (see Figure 4a for a scale diagram of the HR 5110 binary system). The  $0.39 \pm 0.09$  mas (FWHM) angular size we estimated for the central component in our three-component model (fit to the full set of usable data) corresponds to a linear size of  $(2.6 \pm 0.6) \times 10^{11}$  cm, or  $66\% \pm 20\%$  of the diameter of the K star. The corresponding equivalent brightness temperature<sup>3</sup> for the peak of the central component is  $(2.1_{-0.8}^{+1.4}) \times 10^9$  K. The corresponding brightness temperatures for the peaks of the east and west components, respectively, are  $(1.9_{-0.5}^{+0.6}) \times 10^8$  K and  $(2.1_{-0.7}^{+0.9}) \times 10^8$  K. The inferred brightness temperature for each component is consistent with the gyrosynchrotron emission mechanism (see, e.g., Dulk 1985). Below we discuss the properties of the radio

---

<sup>1</sup>The binary’s semi-major axis,  $a \equiv a_F + a_K$ , is determined straightforwardly via the generalization of Kepler’s third law:  $a = [P^2(M_F + M_K)]^{\frac{1}{3}}$ , where  $a$  is in A.U.,  $P$  is the period in years, and component masses  $M_F$  and  $M_K$  are in  $M_\odot$ . For the purpose of obtaining an angular separation of the binary components to compare with our model fitting results, the values of  $P$  and  $M_F$  can be taken from Table 1, but that of  $M_K$  requires more care, since inconsistent estimates of the mass ratio  $q \equiv \frac{M_K}{M_F}$  have been published by Conti ( $0.28 \pm 0.08$ , 1967) and Eker & Doherty ( $0.54 \pm 0.01$ , 1987). Rather than attempting to reconcile the two inconsistent estimates for  $q$ , we take as the best estimate of  $a$  the average of the  $a$  values computed from each of the two published  $q$  values, respectively  $9.92 \pm 0.21 R_\odot$  and  $10.55 \pm 0.03 R_\odot$ , and take as its standard error half the difference between these two values. Converted to angular units by means of the *Hipparcos* parallax, with allowance for the parallax uncertainty, our best estimate of  $a$  becomes  $1.07 \pm 0.05$  mas.

<sup>2</sup>Estimates of the radius of the K star vary between  $2.2 R_\odot$  (obtained using the 0.47 mas angular diameter of Little-Marenin et al. 1986 and the *Hipparcos* parallax) and  $3.4 R_\odot$  (Eker & Doherty 1987). We take as the best estimate of the diameter of the K star twice the average of these two radius estimates and take as its standard error the difference between the two radius estimates. The resulting best angular diameter estimate is  $0.59 \pm 0.12$  mas.

<sup>3</sup>We use the formula for the brightness temperature of a Gaussian source model given in Hjellming (2000).



emission of each of the extended and compact regions further.

How do our results compare with previous VLBI results for HR 5110? Prior VLBI observations of this system were made at epochs when radio emission was nearly quiescent (Lestrade et al. 1984), as well as when the radio emission was relatively strong (Mutel et al. 1985; Little-Marenin et al. 1986). Lestrade et al. observed HR 5110 at 8.4 GHz with a four-element VLBI array on 1982 December 19 when the VLBI-determined flux density of the star was  $\sim 30$  mJy. They found a maximum source size of 1.4 mas (FWHM) by fitting a single circular Gaussian component to their data. The inferred lower bound on the peak brightness temperature of this component is  $2.8 \times 10^8$  K according to the formula of Hjellming (2000). Comparing the size and brightness temperature of the component observed by Lestrade et al. to that of the single elliptical Gaussian component in our one-component model (fit to the full set of usable data), we find that the  $1.66 \pm 0.21$  mas (FWHM) major axis size of our single component is slightly larger than the circular size of the single Lestrade et al. component, and the corresponding  $(4.3^{+2.2}_{-1.3}) \times 10^8$  K brightness temperature of our single component is consistent with the lower bound on the brightness temperature of their single component. Mutel et al. observed HR 5110 at 5.0 GHz with a six-element array on 1983 July 26 when the total flux density of the star varied between 130 and 170 mJy. They found a source size of 1.0 mas (FWHM) by fitting a single circular Gaussian component to their data, which implies a peak brightness temperature of approximately  $7 \times 10^9$  K (again following Hjellming 2000). The values for the size and brightness temperature of this component lie between those we estimated for the single extended component in our one-component model and the compact central component in our three-component model, but closer to those for the central component in our three-component model. Little-Marenin et al. observed HR 5110 at 5.0 GHz with a two-element VLBI array on 1981 April 6 during a decay phase of a strong radio flare. The total flux density during their observation was approximately 200 mJy. They estimated a source size of 3.7 mas by directly comparing the correlated flux density on their single VLBI baseline to the total flux density from single-dish observations made at the same time by Feldman (1983) and assuming a single Gaussian component. This size is approximately twice as large as that we measured for our extended region. Though the size estimate of Little-Marenin et al. is sensitive to any discrepancies between the flux density scales of the VLBI and single-dish observations, we doubt that such discrepancies can explain the large difference between the two measurements. Thus we believe it probable that there is significant variability in the size of this region.

How does the source structure we observed for HR 5110 compare to what has been observed with VLBI for other close binary systems? Our images and Gaussian models provide evidence that a radio core-halo structure was present in HR 5110 during our observations. The size, relative to the diameter of the K star, and brightness temperature of our compact

source are each consistent with the values characteristic of core emission as given by Mutel et al. (1985). Similarly, the size, relative to the binary separation, and brightness temperature of our extended source are each consistent with the values they give for halo emission. A core-halo structure has also been observed for the two RS CVn systems UX Arietis (Mutel et al.) and HR 1099 (Ransom et al. 2002) and for the close binary in Algol (Mutel et al.) during periods when each system was in a decay phase of a radio flare. Mutel et al.’s model for simultaneous core and halo emission describes a system that is in the decay phase of a flare. In our case, the core-halo structure was apparently observed during the onset of a radio flare. However, we cannot exclude the possibility that the flare rise we observed is superimposed upon a decay phase of an earlier flare, because there is no record of the flux density history of HR 5110 immediately before our observations.

What can we infer from the time variability of each of the emission regions identified in our images? Our three-component models indicate that, over the  $\sim 5$  hour period separating the midpoints of intervals 1 and 2, the flux density of the central component increased by  $13.2 \pm 5.2$  mJy ( $92\% \pm 36\%$ ) while the flux densities of the eastern and western components remained roughly constant. In addition, we note that the sizes of each of the three components remained essentially unchanged, meaning that the brightness temperature of only the central component increased, namely about twofold. This result suggests that the compact emission region in our images was located at, or close to, the site of flare activity during the observations. However, the full picture is unclear, because the  $17.5 \pm 7.6$  mJy increase in the combined flux density of all three components in our three-component models does not account for the  $\sim 40$  mJy total flux density increase measured with the VLA between the midpoints of intervals 1 and 2 (even when the VLBI flux density scale is brought into agreement with the VLA scale). The discrepancy is probably due to our model not fully representing the structure of the source. Nevertheless, the increase in the flux density of the compact central component relative to the combined flux density in all three components of our three-component models (from  $\sim 40\%$  to  $\sim 53\%$ ), together with the observed decrease in the total fractional circular polarization (from  $\sim 10\%$  to  $2.5\%$ ) over the course of our observations, is consistent with the interpretation that we are observing a core-halo structure. The core-halo model used by Umana et al. (1993), to reproduce their observed radio spectra for HR 5110, predicts that at 8.4 GHz the core emission is optically thick while the halo emission is optically thin. Since optically thick gyrosynchrotron sources are expected to have a low degree of circular polarization ( $\leq 20\%$  for  $\theta \geq 20^\circ$  and  $\leq 8\%$  for  $\theta \geq 60^\circ$ , where  $\theta$  is the angle between the magnetic field and the line of sight to the observer; Dulk & Marsh 1982), an increase in the relative strength of the core emission compared to the halo emission would result in a decrease in the total fractional circular polarization of the combined source, consistent with our findings.

Over any  $\sim 5$  hour period, the two stellar components of the HR 5110 binary system travel about  $30^\circ$  along their orbital paths. The projection on the sky of the stars' separation vector rotates by nearly the same value since the system is viewed close to face-on ( $i \lesssim 13^\circ$ ). The  $22^\circ \pm 14^\circ$  apparent rotation of the extended emission region that we found in our one-component models (but not in our three-component models) is thus consistent with the system being tidally locked (see also Ransom et al. 2002 in which the radio structure of HR 1099 was found to possibly corotate with the stars in that binary system). If the observed projected rotation is real, and if the extended emission region is indeed fixed with respect to the two stars of the binary system, then we can infer that the direction of rotation of the system is counterclockwise. More observations are needed to study a possible rotation of the radio structure of HR 5110 in detail.

Can we infer the locations with respect to those of the stars within the HR 5110 binary system of each of the compact and extended emission regions seen in our images and Gaussian models? In contrast to multi-epoch astrometric VLBI studies of close binary systems (e.g., Lestrade et al. 1993; Lestrade 1996), a single VLBI epoch gives no definitive information about the location within the system of the emission source. However, in some cases for a single epoch, the source structure itself suggests a likely location of emission components with respect to the stellar components of the binary. For example, in the case of the 1996 May 25 observations of HR 1099 by Ransom et al. (2002), the  $\sim 1.7$  mas separation and apparent relative rotation of the two observed compact components suggested two favored alignments within that binary system, namely emission from well separated regions of the cooler K star's corona and emission from both the K and G stars. Our results for HR 5110 do not favor any particular alignment. If, however, we make the reasonable assumption that all the emission we observed on 1994 May 29/30 is centered on the cooler K star in the HR 5110 binary system (note that F-type stars have not been observed to produce radio emission with flux density  $\gtrsim 0.6$  mJy; Güdel, Schmitt, & Benz 1995), then the alignment would be approximately as illustrated in Figure 4*a,b*. A possible scenario which accounts for the compact and extended emission regions we observed during our observations might then be as follows: Our observations began near the start of a radio flare that originated near the surface of the chromospherically active K star. Particle acceleration accompanying the flare gave rise to the compact central component we found in our three-component Gaussian models, namely one with an angular size of  $0.4 \pm 0.1$  mas (FWHM), or  $66\% \pm 20\%$  the diameter of the K star. As our observations continued, additional particle acceleration by the flare led to an increase in the flux density of HR 5110 from a nearly quiescent level to levels typical of active emission periods. Emission from other energetic particles, possibly originating from earlier flaring on the K star (see, e.g., Mutel et al. 1985; Franciosini & Chiuderi-Drago 1995), and now trapped within the extended magnetosphere of the K star,

or, perhaps, within the interconnected magnetospheres of both the K and F stars, accounts for the two outer components in our three-component models.

## 6. CONCLUSIONS

Here we summarize our findings:

1. During our observations on 1994 May 29/30, the flux density of HR 5110 in right circular polarization rose from  $\sim 33$  mJy to  $\sim 95$  mJy.
2. The radio emission was  $9.6\% \pm 1.4\%$  right circularly polarized during the first hour of observations, and  $2.5\% \pm 0.6\%$  right circularly polarized during the last hour.
3. Our VLBI images suggest an emission region with core-halo structure, i.e., a compact region approximately at the center of an extended region.
4. When we fit a three-component model consisting of three circular Gaussian components to our data, the estimated diameter of the central component was  $0.39 \pm 0.09$  mas (FWHM), or  $66\% \pm 20\%$  of the diameter of the chromospherically active K star in the binary system. The diameter of this component remained essentially unchanged over the course of the observations. In contrast, its flux density and brightness temperature nearly doubled during the observations, suggesting that the central component was at or near the site of flare activity.
5. The two outer components in our three-component model define an extended region  $1.95 \pm 0.22$  mas in its longest dimension oriented at a position angle between  $50^\circ$  and  $70^\circ$ . This region is  $1.8 \pm 0.2$  times the separation of the centers of the K and F stars. The flux densities of each of the outer components remained roughly constant during the observations.

ACKNOWLEDGMENTS. We thank Adam Jeziak and Jerusha Lederman for help with the three-dimensional illustration of the HR 5110 binary system. This research was primarily supported by NASA, through contracts with Stanford University, and by the Smithsonian Institution and York University. Research at York University was partly supported by NSERC. NRAO is operated by Associated Universities, Inc., under cooperative agreement with NSF. The DSN is operated by JPL/Caltech, under contract with NASA. We have made use of the Astrophysics Data System Abstract Service, created by SAO and supported by NASA.

## REFERENCES

- Baars, J. W. M., Genzel, R., Pauliny-Toth, I. I. K., & Witzel, A. 1988, *A&A*, 61, 99
- Conti, P. S. 1967, *ApJ*, 149, 629
- Diamond, P. J. 1995, in ASP Conf. Ser. 82, *Very Long Baseline Interferometry and the VLBA*, ed. J. A. Zensus, P. J. Diamond, & P. J. Napier (San Francisco: ASP), 227
- Dulk, G. A. 1985, *ARA&A*, 23, 169
- Dulk, G. A., & Marsh, K. A. 1982, *ApJ*, 259, 350
- Eker, Z., & Doherty, L. R. 1987, *MNRAS*, 228, 869
- Feldman, P. A. 1983, in IAU Colloq. 71, *Activity in Red-Dwarf Stars*, ed. P. B. Byrne & M. Rodono (Dordrecht: Reidel), 407
- Florkowski, D. R., Johnston, K. J., Wade, C. M., & de Vegt, C. 1985, *AJ*, 90, 2381
- Franciosini, E., & Chiuderi-Drago, F. 1995, *A&A*, 297, 535
- Güdel, M., Schmitt, J. H. M. M., & Benz, A. O. 1995, *A&A*, 302, 775
- Hall, D. S. 1976, in IAU Colloquium 29, *Multiple Periodic Variable Stars*, ed. W. S. Fitch (Dordrecht: Reidel), 287
- Hjellming, R. M. 2000, in *Allen's Astrophysical Quantities*, ed. A. N. Cox (4th ed.; New York: Springer), 121
- Lestrade, J.-F., Mutel, R. L., Preston, R. A., Scheid, J. A., & Phillips, R. B. 1984, *ApJ*, 279, 184
- Lestrade, J.-F., Phillips, R. B., Hodges, M. H., & Preston, R. A. 1993, *ApJ*, 410, 808
- Lestrade, J.-F. 1996, in IAU Symposium no. 176, *Stellar Surface Structure*, ed. K. G. Strassmeier & J. L. Linsky (Dordrecht: Kluwer), 173
- Lestrade, J.-F., et al. 1999, *A&A*, 344, 1014
- Little-Marenin, I. R., Simon, T., Ayres, T. R., Cohen, N. L., Feldman, P. A., Linsky, J. L., Little, S. J., & Lyons, R. 1986, *ApJ*, 303, 780
- Mayor, M., & Mazeh, T. 1987, *A&A*, 171, 157

- Mutel, R. L., Lestrade, J.-F., Preston, R. A., & Phillips, R. B. 1985, *ApJ*, 289, 262
- Mutel, R. L., Morris, D. H., Doiron, D. J., & Lestrade, J.-F. 1987, *AJ*, 93, 1220
- Mutel, R. L., Molnar, L. A., Waltman, E. B., & Ghigo, F. D. 1998, *ApJ*, 507, 371
- Perryman, M. A. C. 1997, *The Hipparcos and Tycho Catalogues* (Noordwijk: ESA)
- Ransom, R. R., Bartel, N., Bietenholz, M. F., Ratner, M. I., Lebach, D. E., Shapiro, I. I., & Lestrade, J. F. 2002, *ApJ*, 572, 487
- Slettebak, A. 1955, *ApJ*, 121, 653
- Turneaure, J. P., Everitt, C. W. F., & Parkinson, B. W. 1986, in *Proc. Fourth Marcel Grossman Meeting on General Relativity*, ed. R. Ruffini (Amsterdam: Elsevier), 411
- Umana, G., Trigilio, C., Hjellming, R. M., Catalano, S., & Rodonó, M. 1999, *A&A*, 267, 126
- Walker, R. C. 1999, in *ASP Conf. Ser. 180, Synthesis Imaging in Radio Astronomy II*, ed. G. B. Taylor, C. L. Carilli, & R. A. Perley (San Francisco: ASP), 433
- Willson, R. F., & Lang, K. R. 1987, *ApJ*, 312, 278

Table 1. Properties and Orbital Elements of HR 5110

Parameter	Value		Reference
RA <sup>a</sup> (h m s; J2000)	13 34 47.74631±0.000036		1
Dec <sup>a</sup> ( <sup>o</sup> ' " ; J2000)	37 10 56.77936±0.00040		1
Trig. Parallax (mas)	22.46±0.62, 22.21±0.45		1,2
Distance (pc)	44.5±1.3, 45.0±0.9		1,2
Orbital Elements: <sup>b</sup>			
$a \sin i$ ( $10^{11}$ cm) <sup>c</sup>	0.40	0.75	3
$a \sin i$ (mas) <sup>d</sup>	0.06	0.11	
$P$ (days)	2.613214±0.000003		4
$i$ ( <sup>o</sup> )	8.9		3
$e$	0		3
$\omega$	–		
$\Omega$	(Not Determined)		
$T_{conj}$ (HJD) <sup>e</sup>	2445766.655±0.013		3
Stellar Properties: <sup>b</sup>			
Spectral Type	F2 IV	K0 IV	5,6 <sup>f</sup>
Mass ( $M_{\odot}$ )	1.5	0.8 <sup>c</sup>	3
Radius ( $R_{\odot}$ )	2.6 <sup>g</sup>	3.4 <sup>h</sup>	3
Radius (mas) <sup>d</sup>	0.27	0.36	

References. — 1. *Hipparcos* Catalogue (Perryman 1997); 2. VLBI (Lestrade et al. 1999); 3. Eker & Doherty 1987; 4. Mayor & Mazeh 1987; 5. Slettebak 1955; 6. Little-Marenin et al. 1986

<sup>a</sup>The *Hipparcos* (J2000) coordinates are for epoch 1991.25.

<sup>b</sup>Two entries correspond to the two stars of the binary system.

<sup>c</sup>Using  $1.5 M_{\odot}$  for the mass of the F star, and the mass ratio  $q \equiv \frac{M_K}{M_F} = 0.54 \pm 0.01$  (Eker & Doherty 1987), we then obtain the mass of the K star. We note here that Conti 1967 found a significantly different value for the mass ratio of the system:  $q = 0.28 \pm 0.08$ . This value leads to a larger estimate of the inclination of the orbit,  $i = 13.2^{\circ}$ , but does not significantly affect the semi-major axis of the binary,  $a = a_F + a_K$ , since  $a \propto (M_F + M_K)^{\frac{1}{3}}$ .

<sup>d</sup>For a distance of 44.5 pc.

<sup>e</sup>Heliocentric time of conjunction with the K star in front.

<sup>f</sup>Note also inference of K2 IV by Eker & Doherty 1987.

<sup>g</sup>Modified using the *Hipparcos* parallax.

<sup>h</sup>Radius of the K star in the limit of filling its Roche lobe. We note that the mass ratio,  $q = 0.28 \pm 0.08$ , found by Conti 1967 leads to a smaller value for the Roche lobe radius of the K star:  $2.6 R_{\odot}$ . This radius is more consistent with the angular diameter of the K star found by Little-Marenin et al. 1986: 0.47 mas.

Table 2. VLBI Observations of HR 5110

Observing Date	Total Time <sup>a</sup> (hours)	Source	Dwell Time (min. per 10 min. cycle)	Antennas <sup>b</sup>
1994 May 29/30	12.8	HR 5110	2.0	Aq,Eb,Gb,Go,Ro,Y27,Hn
		J1340+379	1.3	
		J1334+371	1.7	
		J1328+363	0.8	

<sup>a</sup>Total length of the observing run.

<sup>b</sup> Aq = 46m, ISTS (now CRESTech/York Univ.), Algonquin Park, Ontario, Canada; Eb = 100m, MPIfR, Effelsberg, Germany; Gb = 43m, NRAO, Green Bank, WV, USA; Go = 70m, NASA-JPL, Goldstone, CA, USA; Ro = 70m, NASA-JPL, Robledo, Spain; Y27 = phased VLA equivalent diameter 130m, NRAO, near Socorro, NM, USA; Hn = 25m, NRAO, Hancock, NH, USA (one of the 10 antennas comprising the VLBA).

Table 3. One-Component Model Parameters for HR 5110

Interval (UT)	$S$ (mJy)	Elliptical Gaussian <sup>a</sup>		p.a. (deg)
		Major Axis (mas)	Axial Ratio	
(1)	(2)	(3)	(4)	(5)
full	$39.6 \pm 1.9$	$1.66 \pm 0.21$	$0.58 \pm 0.17$	$64 \pm 8$
22:00–26:50	$33.0 \pm 2.5$	$1.67 \pm 0.24$	$0.59 \pm 0.21$	$63 \pm 10$
26:50–32:00	$56.4 \pm 4.9$	$1.77 \pm 0.23$	$0.58 \pm 0.21$	$85 \pm 10$

<sup>a</sup>The center of the elliptical Gaussian component is fixed at the phase center.

Note. — The description of the column entries is given below. The standard errors were estimated using the procedure described in §3.

(1) Data interval with respect to 0 UT, 1994 May 29 (full  $\equiv$  full usable time range, 22:00–32:00 UT).

(2) Flux density of the elliptical Gaussian component.

(3) FWHM of the major axis of the Gaussian component.

(4) Axial ratio of the Gaussian component.

(5) Position angle (east of north) of the major axis of the Gaussian component.



Table 4. Three-Component Model Parameters for HR 5110

Interval (UT)	Center <sup>a</sup>		West				East			
	<i>S</i> (mJy)	FWHM (mas)	<i>S</i> (mJy)	FWHM (mas)	Rad (mas)	$\theta$ (deg)	<i>S</i> (mJy)	FWHM (mas)	Rad (mas)	$\theta$ (deg)
(1)	(2)	(3)	(4)	(5)	(6)	(7)	(8)	(9)	(10)	(11)
full	$18.6 \pm 2.7$	$0.39 \pm 0.09$	$10.3 \pm 2.2$	$0.91 \pm 0.13$	$0.51 \pm 0.10$	$-118 \pm 7$	$9.5 \pm 1.3$	$0.92 \pm 0.11$	$0.50 \pm 0.10$	$58 \pm 9$
22:00–26:50	$14.4 \pm 2.8$	$0.39 \pm 0.09$	$10.8 \pm 2.5$	$0.93 \pm 0.13$	$0.49 \pm 0.13$	$-119 \pm 9$	$9.6 \pm 2.6$	$0.92 \pm 0.16$	$0.53 \pm 0.13$	$59 \pm 11$
26:50–32:00	$27.6 \pm 4.4$	$0.40 \pm 0.10$	$14.4 \pm 3.4$	$0.88 \pm 0.14$	$0.54 \pm 0.14$	$-122 \pm 12$	$10.3 \pm 2.5$	$0.87 \pm 0.20$	$0.46 \pm 0.14$	$55 \pm 11$

<sup>a</sup>The center of the central circular Gaussian component is fixed at the phase center.

Note. — The description of the column entries is given below. The standard errors were estimated using the procedure described in §3.

- (1) Data interval with respect to 0 UT, 1994 May 29 (full  $\equiv$  full usable time range, 22:00–32:00 UT).
- (2) Flux density of the central circular Gaussian component.
- (3) Size (FWHM) of the central circular Gaussian component.
- (4) Flux density of the western circular Gaussian component.
- (5) Size (FWHM) of the western circular Gaussian component.
- (6,7) Location (radial distance and position angle, respectively) of the western circular Gaussian component.
- (8) Flux density of the eastern circular Gaussian component.
- (9) Size (FWHM) of the eastern circular Gaussian component.
- (10,11) Location (radial distance and position angle, respectively) of the eastern circular Gaussian component.

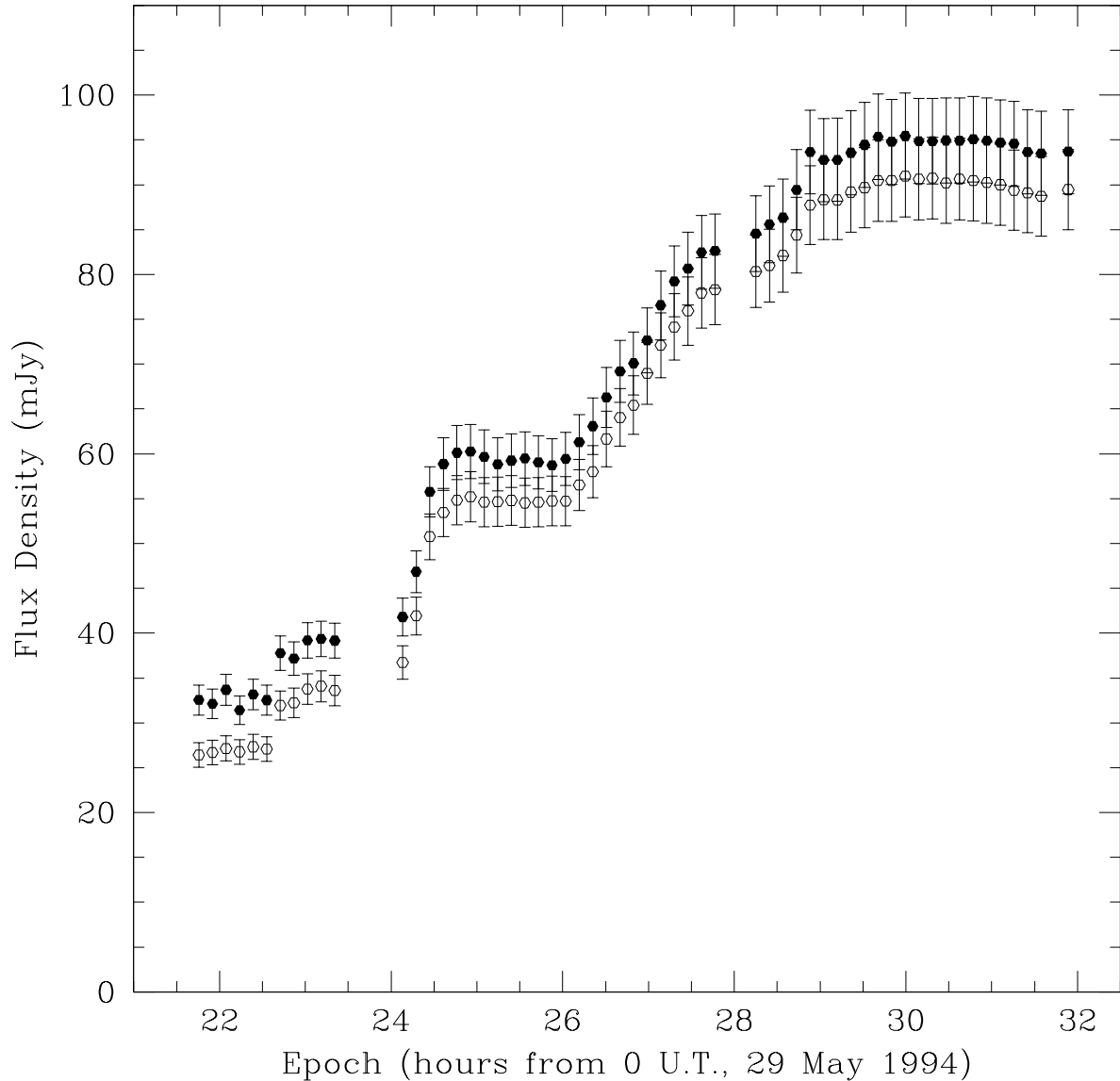


Fig. 1.— VLA radio light curve of HR 5110 at 8.4 GHz in RCP (filled circles) and LCP (open circles) for 1994 May 29/30. (Note that the VLBI observations for this session were in RCP only.) The averaging interval is 10 minutes, the period of our observing cycle. The uncertainties shown include standard errors derived from the internal scatter of the VLA data but are dominated by the 5% systematic contribution that we allowed for the error in flux density calibration of the VLA data. The relative accuracy is much higher if, as expected, the VLA calibration error is not strongly time variable.

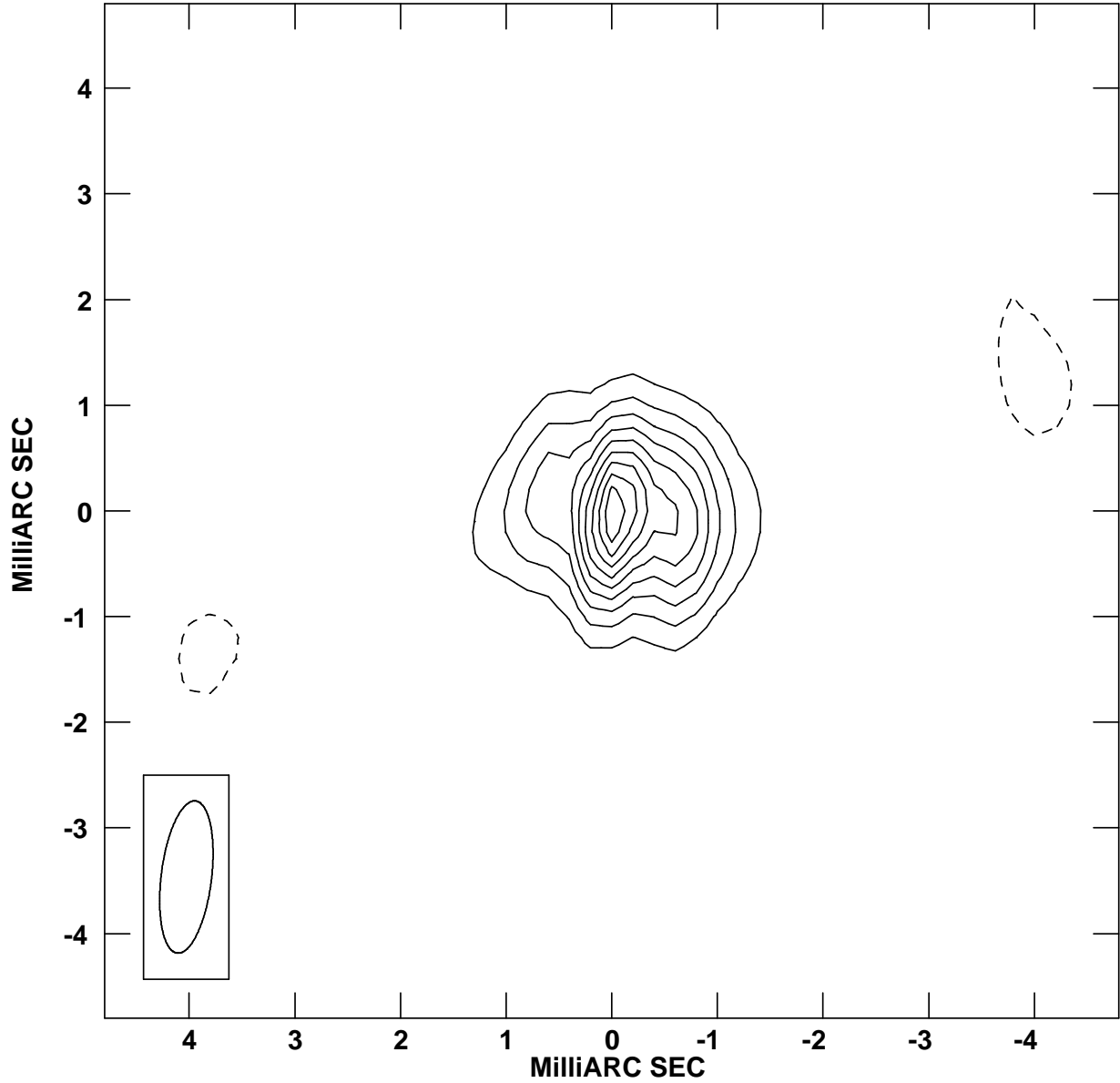


Fig. 2.— VLBI image of HR 5110 for 1994 May 29/30. Here and hereafter, north is up and east to the left. The FWHM beam size is  $1.5 \times 0.5$  mas oriented at  $-7^\circ$  and is shown at the lower left. The contour levels are -10, 10, 20, 30, 40, 50, 60, 70, 80, and 90% of the peak brightness of 14.6 mJy/beam. The background rms noise level is 0.47 mJy/beam. The total CLEAN flux density in the image is 34.1 mJy.

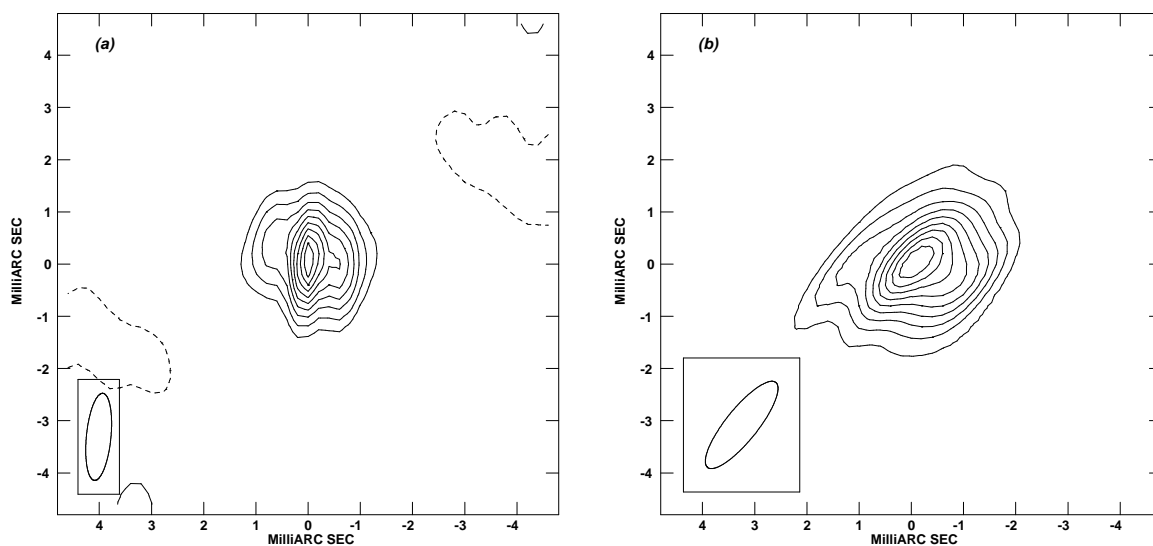
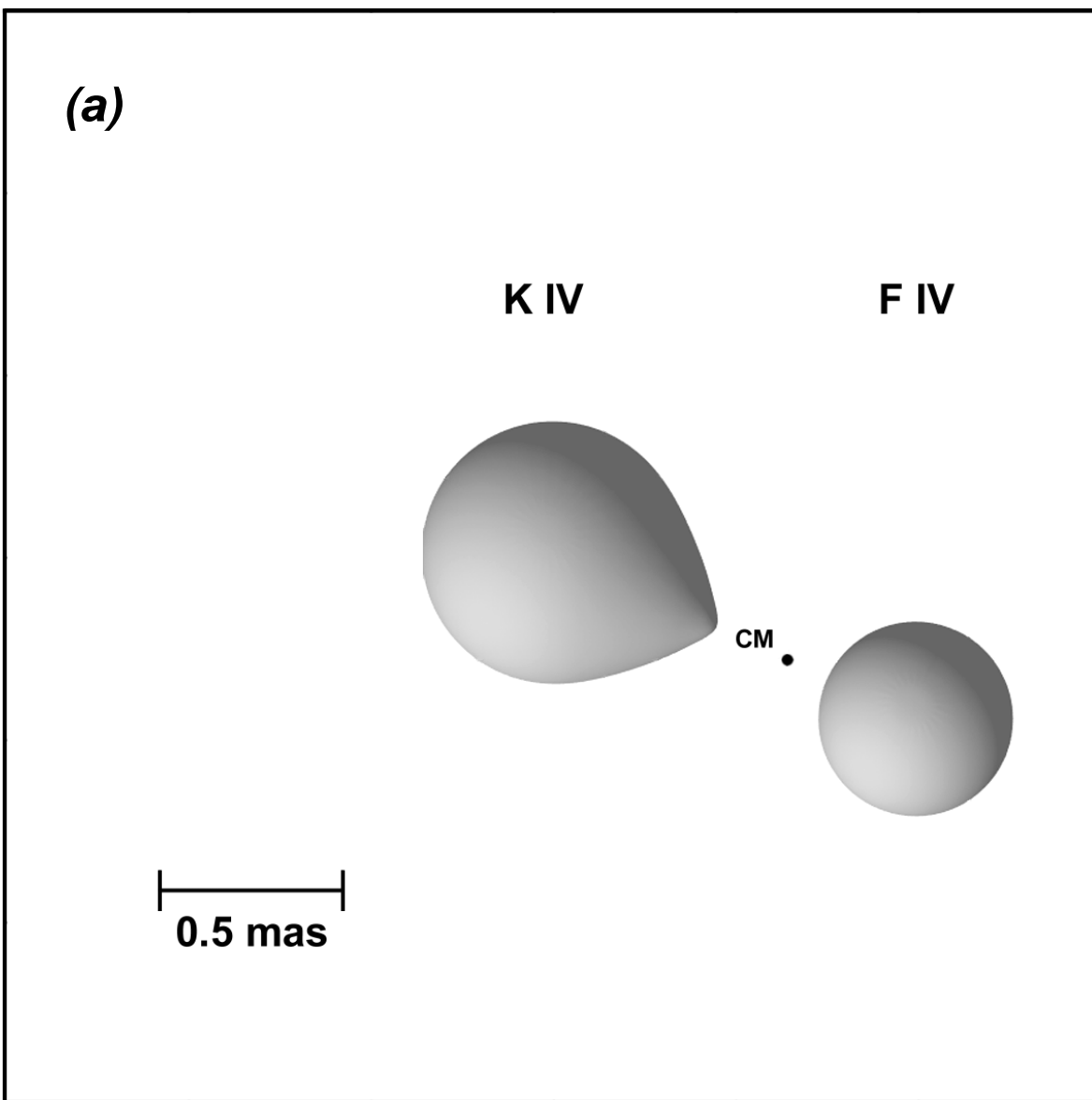


Fig. 3.— VLBI images of HR 5110 for (a) the first half and (b) the second half of the 1994 May 29/30 observations. The contour levels displayed for each image are -10, 10, 20, 30, 40, 50, 60, 70, 80, and 90% of the peak brightness for that image. The exact time interval, FWHM beam size and orientation, peak brightness, background rms noise, and total CLEAN flux density for each image are:

(a) Interval 1: 1994 May 29/22:00–30/02:50 UT;  $1.7 \times 0.5$  mas at  $-6^\circ$ ; 12.6 mJy/beam; 0.50 mJy/beam; 30.1 mJy.

(b) Interval 2: 1994 May 30/02:50–08:00 UT;  $2.1 \times 0.6$  mas at  $-39^\circ$ ; 21.2 mJy/beam; 0.39 mJy/beam; 57.8 mJy.



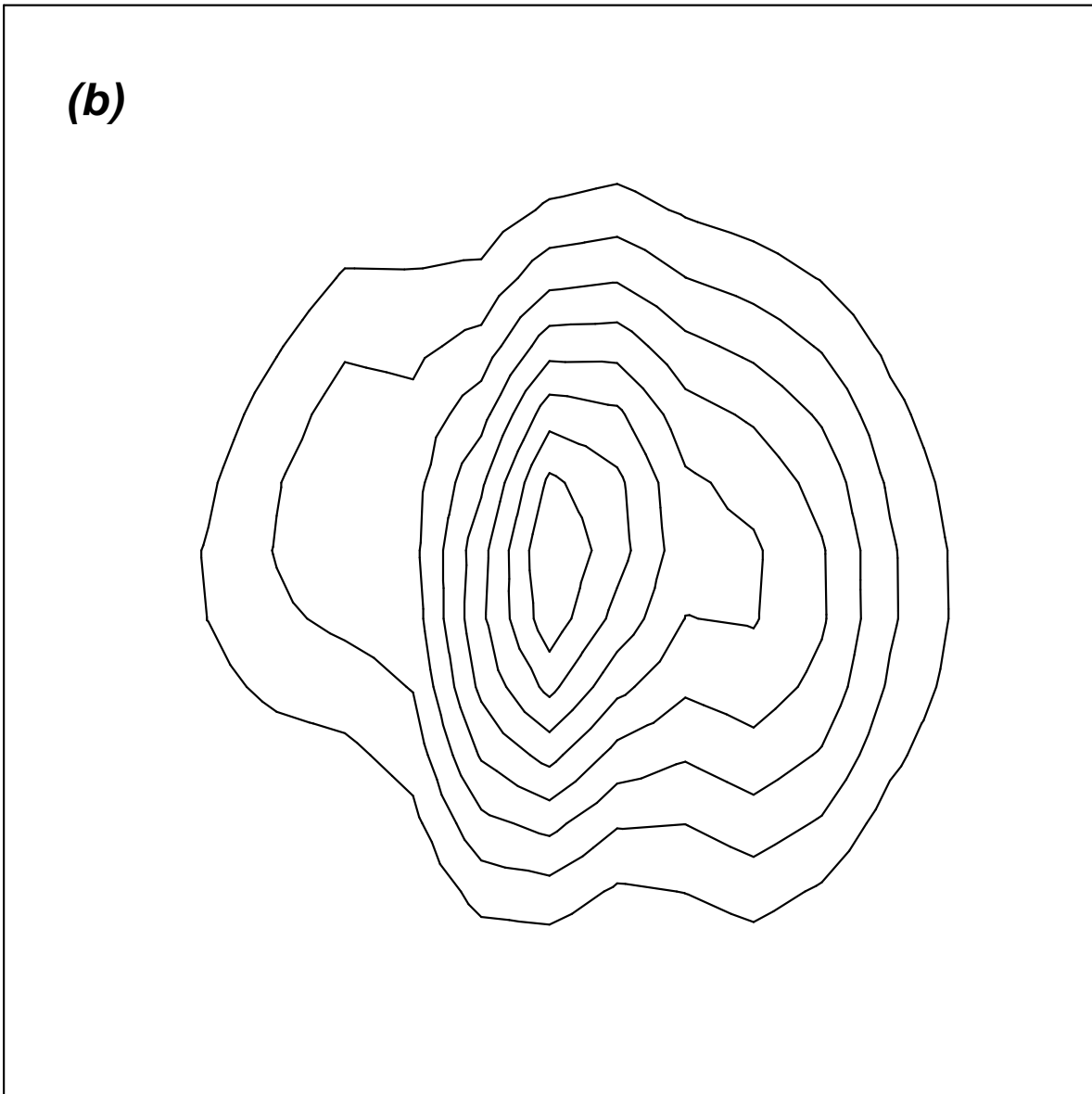


Fig. 4.— (a) An artist’s three-dimensional rendering of the HR 5110 binary system as seen from Earth, for the orbital elements and stellar parameter values in Table 1. The scale bar is for a system distance of 44.5 pc. The point labeled “CM” is the center of mass of the binary system. The system is shown at the midpoint of our observations. From the time of conjunction and the orbital period given in Table 1, we calculate the phase to be  $0.39 \pm 0.02$ . (Note that conjunction with the F star in front occurs at phase 0.25.) The position angle of the line connecting the stars’ centers and starting at the F star is  $65^\circ$  in this rendering; i.e., approximately equal to the position angle of the extended component in our one-component model for the full session. For this configuration, the position angle of the ascending node,  $\Omega$ , is  $-75^\circ$  if the stars are rotating counterclockwise and  $-155^\circ$  if the stars are rotating clockwise. The placement of the K star northeast, rather than southwest, of the F star is